European Journal of Neuroscience, Vol. 10, pp. 95–105, 1998

Role of the cerebellum in reaching movements in humans. II. A neural model of the intermediate cerebellum

Nicolas Schweighofer,[1,2] Jacob Spoelstra, [1] Michael A. Arbib[1] and Mitsuo Kawato[2]
[1]Centre for Neural Engineering, University of Southern California, Los Angeles, CA 90089–2520, USA
[2]ATR Human Information Processing Research Laboratories, 2–2, Hikaridai, Seika-cho, Soraku-gun, Kyoto 619–02 Japan

Keywords: cerebellar learning, inferior olive, inverse dynamics, motor learning, parallel fibres

Abstract

The cerebellum is essential for the control of multijoint movements; when the cerebellum is lesioned, the performance error is more than the summed errors produced by single joints. In the companion paper (Schweighofer *et al.*, 1998), a functional anatomical model for visually guided arm movement was proposed. The model comprised a basic feedforward/feedback controller with realistic transmission delays and was connected to a two-link, six-muscle, planar arm. In the present study, we examined the role of the cerebellum in reaching movements by embedding a novel, detailed cerebellar neural network in this functional control model. We could derive realistic cerebellar inputs and the role of the cerebellum in learning to control the arm was assessed.

This cerebellar network learned the part of the inverse dynamics of the arm not provided by the basic feedforward/feedback controller. Despite realistically low inferior olive firing rates and noisy mossy fibre inputs, the model could reduce the error between intended and planned movements. The responses of the different cell groups were comparable to those of biological cell groups. In particular, the modelled Purkinje cells exhibited directional tuning after learning and the parallel fibres, due to their length, provide Purkinje cells with the input required for this coordination task. The inferior olive responses contained two different components; the earlier response, locked to movement onset, was always present and the later response disappeared after learning. These results support the theory that the cerebellum is involved in motor learning.

Introduction

An essential property of movement coordination is the ability to compensate for the interaction torques arising during a reaching movement, and recent data have shown that the cerebellum is involved in this compensation (Bastian *et al.*, 1996). In the companion paper (Schweighofer *et al.*, 1998), detailed analysis suggests that the cerebellum forms part of the inverse model of the arm: the motor cortex is an approximate inverse model and the cerebellum is the locus of the part of the inverse dynamics specifically involved in compensating for the interaction torques. In the present paper, a novel computational model of the cerebellum was developed and used to test the validity of this hypothesis.

The neural circuitry in the cerebellar cortex is very uniform and the cerebellum itself can be analysed in terms of small structural and functional units inserted into various extracerebellar systems. These units are called microcomplexes (Ito, 1984) and each is composed of a cerebellar microzone and a small number of nuclear cells. A microzone receives two primary inputs, mossy fibres and climbing fibres, and the output is carried by axons of the deep nuclear cells. Oscarsson (1980) defined the microzone as a narrow longitudinal zone in the cerebellar cortex receiving climbing fibres from a small group of inferior olive (IO) neurones and associated with a unique bodily function (e.g. the detection of a particular noxious stimulus). Indeed, the IO, which gives rise to the climbing fibres, is divided into clusters of electrotonically coupled cells having the same functionality that fire with some synchrony (Llinás *et al.*, 1974). The set of mossy fibre inputs to the microcomplex, relayed to the cerebellar cortex by the granule cells and their parallel fibres, is characterized by its considerable divergence across many other microzones.* This set constitutes a general context for sensorimotor action; that is, a large set of signals providing information about the state of activity of various structures, from higher levels to sensory ones. The granule cells are known to have excitatory projections to the Purkinje cells and to the inhibitory interneurones (basket, stellate and Golgi cells) of the cerebellar cortex. The Golgi cells feedback on to the granule cells via highly efficacious synapses that have long-lasting effects. The stellate cells inhibit adjacent Purkinje cell dendritic trees, and the basket cells send long axons (perpendicular to the parallel fibres) that connect the soma of several Purkinje cells. Because Purkinje

*The number of neurones, the divergence and convergence values were found in Ito (1984).

Correspondence: Nicolas Schweighofer, ERATO, Kawato Dynamics Brain Project, 2–2, Hikaridai, Seika-cho, Soraku-gun, Kyoto 619–02 Japan. E-mail: nicolas@erato.atr.co.jp

Received 9 December1996, revised 29 April 1997, accepted 15 July 1997

cells inhibit nuclear cells, while the collaterals of some mossy fibres excite the nuclear cells, nuclear cell activity is modulated by the microzone activity. Because the Purkinje cells of the intermediate cerebellum project to the interpositus nucleus, which itself projects to the motor cortex via the thalamus and to the spinal cord via the red nucleus, they have a major role in controlling ongoing movements.

The highly regular structure of the cerebellum has lent itself to numerous modelling studies for more than 25 years, both theoretical and computational. The first theoretical models were based on proposals of Marr (1969) and Albus (1971) that the cerebellum is an array of perceptrons (the Purkinje cells) that receive their inputs from a large set of granule cells. The granule cell population acts as an expansion recoder, which dramatically improves the learning capabilities of the Purkinje cells. Albus' model was of great importance because it predicted the existence of long-term depression (LTD) due to concurrent activation of climbing fibre and granule cell inputs, later discovered experimentally by Ito (1984). Boylls' computer model (1975) introduced 'leaky integrator' neurones to model the short-term effect of climbing fibres on cerebellar neurones. This model was the first to address the real-time processing capabilities of the Golgi cell – granule cell complex. The work of Fujita (1982) combined the dynamic, real-time behaviour of the cerebellar circuitry with the plasticity in the cerebellar cortex, successfully accounting for several features of the vestibulo-ocular reflex. Thompson (1986) proposed an integrative theoretical model for the role of the cerebellum in classical conditioning in which all known aspects of cerebellar function involved in classical conditioning are taken into account. Thach *et al*. (1992) proposed a theoretical model for movement coordination in which coordination is due to the groups of Purkinje cells linked by parallel fibres. Garwicz & Andersson (1992) showed that there is indeed a spread of activity along the parallel fibres, as predicted. In this approach, groups of cortical cells project to specific groups of nuclear cells, which may influence the synergetic muscles across several joints in the limb. Berthier *et al*. (1993) implemented a cerebellar model for arm control that includes the neurochemical chain of events leading to LTD, first proposed by Houk *et al*. (1990). Neuronal coding is simplified and no arm dynamics is incorporated in this model, however. Kawato & Gomi (1992) and Miall *et al*. (1993) proposed theoretical cerebellar models dealing with plant dynamics control. These models appear to reproduce accurately several movements, but they do not take into account detailed cerebellar anatomy, neurophysiology, or neurochemistry. Schweighofer *et al*. (1996a,b) implemented a detailed cerebellar model for saccade control and adaptation. This large, realistic cerebellar network of neurone-like units allows the study of the complex spatio-temporal behaviour of neuronal subpopulations implicated in saccadic control and adaptation. Although this model accounts for three types of mossy fibre inputs and delayed IO spikes, the plant is simplified (no dynamics is included) and only one degree of freedom is considered.

The present study utilized a novel, large, realistic computer model of the intermediate cerebellum embedded in the functional anatomical model for visually guided arm movement proposed in the companion paper. The model accounts for arm dynamics, arm muscles, significant delays, and behavioural, anatomical and neurophysiological findings. The strength of this novel approach is that it bridges the gap between functional/anatomical models (Thach *et al.*, 1992), learning models (Marr, 1969; Albus, 1971; Thompson, 1986; Houk *et al.*, 1990), and control models (Kawato & Gomi, 1992). This model includes 'temporal neurones' (Boylls, 1975) and is based on feedback error learning (Kawato *et al.*, 1987), but differs in that it accounts for the fact that the motor cortex is well suited to control single joint movements (Evarts, 1966; Cheney & Fetz, 1980) and that the cerebellum may learn how to adjust motor commands in a manner specific to multiarticular movements. Because both learning and control are accounted for, the model resembles the models of Fujita (1982), Berthier *et al*. (1993) and Schweighofer *et al*. (1996a,b). However, the present model includes some important new features. First, by incorporating a two-link, six-muscle arm model with realistic neuronal conduction delays, the cerebellum was required to learn how to control and coordinate a non-trivial system. Second, by embedding the model in the functional model described in the companion paper, the issue of dynamics control could be specifically addressed. Third, we constrained the model severely with anatomical, neurochemical and neurophysiological data. Finally, realistic mossy fibres and inferior olive inputs were derived.

The cerebellum neural network

The functional model described in the companion paper is summarized in Fig. 1, with the addition of the IO, the role of which is crucial for the cerebellar model.

The mossy fibre inputs

As reviewed in the companion paper, the intermediate cerebellar cortex receives both mossy fibres from the periphery and from the cerebral cortex. The input mapping in the cerebellar cortex consists of multiple representations of body parts in a pattern called 'fractured somatotopy'. Because the arm model used was a two-joint arm with a total of six muscles, it was not possible to correlate precisely the activity of the mossy fibres of central origin, which was in 'synergy' coordinates, with the sensory mossy fibres, which was in muscle coordinates. This was approximated by superimposing a map with two patches for the mossy fibres (one for each joint) from central origin on a map with six patches (one per muscle) for the sensory mossy fibres. In both, the area from shoulder to elbow was mapped from left to right, but only the sensory map had a specific representation for flexors and extensors. Although the maps were superimposed, each mossy fibre was either a sensory cell or a cell originating from the cerebral cortex. The results of Van Kan *et al*. (1993) show that some mossy fibre firing rates are approximated by a 'saturating ramp' function of the angle and others by a 'ramp' function of the joint velocity. Because cells often carry more than one modality, the input of each cell was modelled by a combination of the variables. The threshold appears to be highly variable for the position and approximately zero for the velocity. Due to the linear relationship between angle and muscle length in the arm model, the input to a sensory mossy fibre is given by:

$$mf\_inp_{sens} = [\mu_1(l - L)]_{\min}^{\max} + [\mu_2 \dot{l}]^+, \quad (1)$$

with $[x]_{\min}^{\max} = x$ if $max < x < min$, min if $x \leqslant min$, and max if $x \geqslant max$, while $[x]^+ = x$ for $x > 0$ and 0 otherwise. l and $\dot{l}$ are delayed muscle length and delayed rate of stretch. A 10-ms delay was included in order to reflect the rapid conduction velocity of the spino-cerebellar tract. L, the average muscle length and μ_1 and μ_2 were generated randomly (uniform distribution) for each cell. The cells of with inputs of central origin are correlated with joint acceleration, velocity, and position:

$$mf\_inp_{des} = [\lambda_1\theta_d + \lambda_2\dot{\theta}_d + \lambda_3\ddot{\theta}_d]^+, \quad (2)$$

with λ_1, λ_2 and λ_3 generated randomly (uniform distribution) between –max and max values. For both type of cells, the membrane potential equation is given by the following linear first order differen-

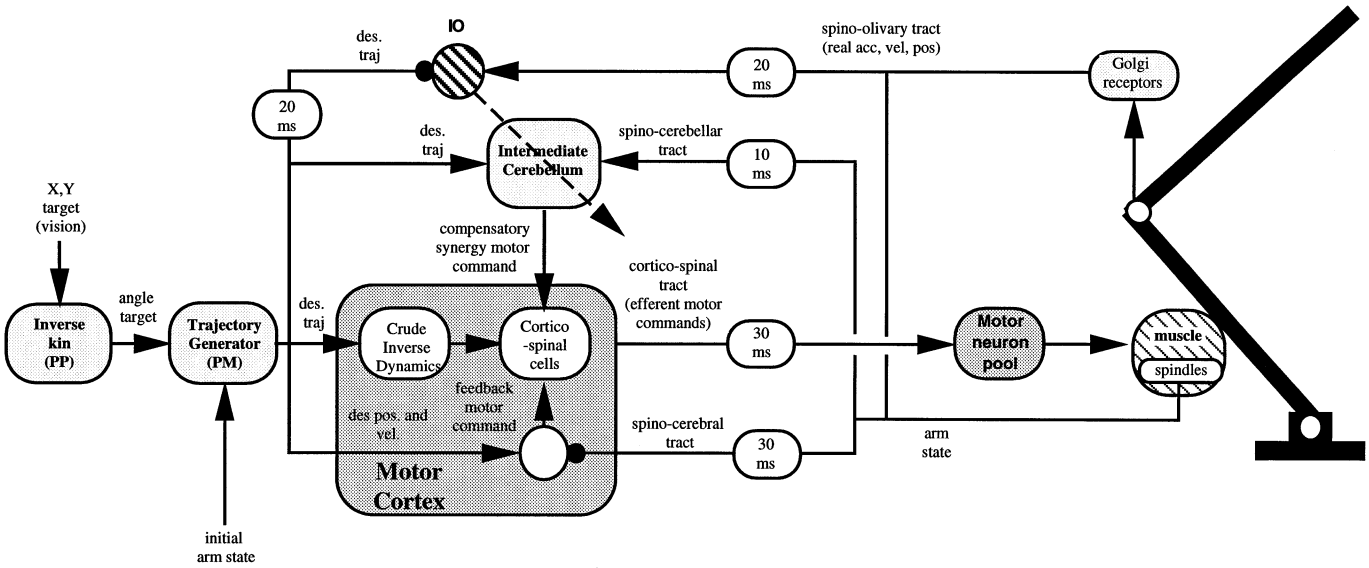

FIG. 1. Functional diagram of the model for on-line control of arm movements described in the companion paper, with the addition of the inferior olive (IO) which computes the feedback error. The delayed desired trajectory (position, velocity, and acceleration) forms the inhibitory inputs to the IO, while the actual, delayed trajectory sensed by spindles and Golgi tendons receptors forms the excitatory input. See Schweighofer *et al*. (1998) for details. PP, posterior parietal cortex; PM, premotor cortex.

tial equation. Refer to Appendix 1 for generic neural modelling used and to Appendix 2 for the parameters used.

$$\tau_{mf} \frac{d\,mf}{dt} = -mf + mf\_inp. \tag{3}$$

The mossy fibre firing rate *MF* is equal to the membrane potential (in this paper, upper case variables represent firing rates, and lower case variables represent membrane potentials). A noise term averaging 10 spikes/s (drawn from a uniform distribution between 0 and 20 spikes/s) was added to the sensory mossy fibre input to reflect the inherent noise of the muscle spindle signal.

The Golgi–granule cell complex

In the cerebellum, each mossy fibre diverges into ⊤ 16 branches, which end in glomeruli. For computational tractability, this divergence number was set at four in the model. Mossy fibre and Golgi cell axon terminals were the presynaptic elements and granule cell dendrites were the postsynaptic elements of the glomeruli. The present model included 81 mossy fibres, and thus, 324 glomeruli. To allow a rich combination of inputs and to reproduce the very large divergence between the mossy fibres and the granule cells, a layer of $54 \times 54 = 2916$ granule cells was modelled, giving a divergence ratio of $2916/81 = 36$ between the mossy fibres and the granule cells. Granule cells have an average of four dendrites, each receiving a distinct mossy fibre input. To reproduce this architecture, a statistical (Gaussian) distribution of glomeruli to granule dendrites was generated. The probability that a glomerulus influenced the four dendrites of a granule cell was proportional to the distance from the granule cell to the glomerulus. There were 2916 granule cells and 11 664 granule cell dendrites connected to the 324 glomeruli in the model, thus, there were 36 granule cell dendrites (each was equivalent to a synapse in the model) per glomerulus. When a granule cell was contacted by only one active mossy fibre, it fired at a very low rate and only multiple active inputs had a significant effect on a granule cell. Because the number of Golgi cell synapses on the glomerulus is presently unknown, it was assumed that three Golgi cell synapses contact each glomerulus. The probability that a Golgi cell synapse influences a glomerulus was proportional to the distance from the centre of the Golgi cell to the glomerulus. The glomeruli thus received a statistical distribution of Golgi cell synapses. This Gaussian connectivity yielded an approximate cone of inhibition.†

The glomerulus activity *GLOM* is defined by:

$$GLOM = \left[MF - \sum_{k=1}^{3} GO\_w(k) \right]^{+}, \tag{4}$$

where *GO_w* is the modified firing rate of a Golgi cell given in equation 7. Because the glomeruli are not neurones but axon terminals, there is no time constant.

The granule cell membrane potential is given by the following equation:

$$\tau_{gc} \frac{d\,gc}{dt} = -gc + \sum_{k=1}^{4} w_{mf\_gc}(k)\ GLOM(k). \tag{5}$$

The sum of the activity of four distinct glomeruli represented the effect of the four granule cell inputs, each weighted by $w_{mf\_gc}(k)$. These weights were chosen from a Gaussian distribution. The firing rate for each granule cell *GC* was computed by applying a sigmoid function as described in Appendix 1.

Granule cell axons are characterized by the long length of the parallel fibres, a decreasing number of synapses along the parallel fibres, and synapses on the ascending branch of the axon. To reproduce the long length of the parallel fibres, it was assumed that they make synaptic contacts with the inhibitory interneurones and Purkinje cells the entire length of the cerebellar patch. To reproduce the decrease of the number of synapses along the parallel fibre, the probability of synaptic contact was drawn from a Gaussian distribution, the standard

†To avoid undesirable edge effects, each neurone layer formed a torus.

deviation of this distribution being an idealized 'parallel fibre length' (also note that in the model and the cerebellum, a parallel fibre contacts a particular Purkinje cell only once). Finally, granule cell–Purkinje cell synapses on the ascending part of the granule cell axon were modelled. The *x–y* coordinates of the granule cells were selected from Gaussian distributions. Note that in the model, all granule cell–Purkinje cell and parallel fibre–Purkinje cell synapses were modifiable and could undergo LTD, but the synapses on inhibitory cells were not modifiable.

Golgi cells receive a sparse distribution (10%) of parallel fibre contacts and mossy fibre inputs from the underlying mossy fibres. Nine Golgi cells were included in the present model, regularly spaced in the cerebellar patch. One glomerulus out of nine connected the Golgi cells. In the model, the upper Golgi dendritic tree had 200 synapses (for simplicity, the dendritic trees were not overlapping). Each Golgi cell projected back to the glomeruli as described above. The membrane potential equation for each Golgi cell is:

$$\tau_{go}\frac{dgo(i)}{dt} = -go(i) + \sum_k w_{gc\_go}GC(k) + \sum_n\sum_m w_{mf\_go}GLOM(n)(m). \quad (6)$$

The firing rate *GO* was obtained by applying a sigmoid function to the membrane potential value. Thus, the Golgi cell acted a priori as a feedforward-feedback inhibitory system acting as a 'cooler' (Albus, 1971), which would prevent the cortex from receiving too much excitation and allow better learning. Golgi cell synapse activity has a timecourse as long as several hundred milliseconds (Eccles *et al.*, 1967). In the present model, Gaussian distributions for the Golgi cell–granule cell synaptic efficacies, and the time constants of the Golgi cell–granule cell synapses were assumed. This led to the granule cells having different phase leads (Boylls, 1975; Fujita, 1982), that is, some were mostly tonic and some mostly phasic. With *GO_w* the modified firing rate of a Golgi cell introduced in equation 5,

$$\tau_w(i)\ \frac{dGO\_w(i,j)}{dt} = -GO\_w(i,j) + w\_go(i)GO(i), \quad (7)$$

with both $\tau_w(i)$ and $w\_go(i)$ generated according to Gaussian distributions.

Purkinje, stellate and basket cells

To approximate the flat structure of the Purkinje cell dendritic tree (the dendritic plate), the modelled cerebellar patch was a 12×3 array, corresponding to three rows and 12 columns of Purkinje cells (because there were four microcomplexes, there were 3×3 Purkinje cells per microcomplex). In the present model, the Purkinje cell somas were distributed in a shifted manner such that one Purkinje cell dendritic plate out of six along the parallel fibre beam was crossed by the same set of parallel fibres. Purkinje cells exhibit a complex electrophysiology with active membrane properties in both the soma and dendrites in response to granule cell–parallel fibre inputs. In the present model, there were 72 dendrites per Purkinje cell, each receiving 10 parallel fibre inputs, one stellate cell input, and two direct granule cell inputs, which corresponded to one vertical synapse for every granule cell. The membrane potential for a dendrite (for simplicity, this is not a differential equation) is:

$$dend = \sum_j w_{ltd\_gc}(j)GC(j) + \sum_j w_{ltd\_pf}(j)PF(j) - w_{stel\_pc}STEL \quad (8)$$

where both w_{ltd} are vectors of adjustable synaptic weights, initially randomly generated, *GC* is the vector of firing rates of the granule cells (this term is due to the ascending portion of the granule cell axon), *PF* is the parallel fibre inputs, and *STEL* is the stellate cell input.‡ The dendrite firing rate *DEND* was calculated by applying a sigmoid function to the dendritic membrane potential, as described in Appendix 1. The Purkinje cell membrane potential at the soma is the sum of the dendrite firing rates. Thus, the Purkinje cell membrane potential equation is given by:

$$\tau_{pc}\ \frac{dpc(i)}{dt} = -pc(i) + \sum_j DEND(j) - w_{ba\_pc}\sum_k BA(k), \quad (9)$$

where *DEND* is the vector of firing rates of the dendrites, *BA*, the basket cell firing rate, and w_{ba_pc}, the strength of the basket cell input.

The hypothesized role of the stellate cells is to prevent saturation of the Purkinje cell dendritic tree when many parallel fibres are active (before the slower Golgi cell-mediated inhibition takes place). The basket cell has the same type of dendritic tree as the stellate cell, but the basket cell axon runs perpendicular to the parallel fibres and inhibits several Purkinje cell somas. It is hypothesized that basket cells provide 'contrast' enhancement by lateral inhibition in the cerebellar cortex. A strongly activated group of parallel fibres strongly excites directly contacted basket and Purkinje cells, while surrounding Purkinje cells are inhibited via basket cell-mediated inhibition. To simplify the present model, only one stellate and one basket cell per Purkinje cell were included. Because parallel fibre–stellate cell and parallel fibre–basket cell connections are sparse, each stellate and basket cell dendritic tree had 100 synapses in the present model. The membrane potentials are given by:

$$\tau_{stel}\ \frac{d\ stel(i)}{dt} = -stel(i) + \sum_j w_{gc\_stel}(j)GC(j) \quad (10)$$

$$\tau_{ba}\ \frac{d\ ba(i)}{dt} = -ba(i) + \sum_j w_{gc\_ba}(j)GC(j) \quad (11)$$

In the simulations, $w_{gc\_ba} = w_{gc\_stel}$.

Interpositus nuclear cells

A microcomplex is defined by a one-to-one relationship between an IO cell group, a well-defined group of nuclear cells, and an overlying microzone. The unidirectional functional change in weights due to LTD (which results in an increase in nuclear output due to the inhibitory nature of the Purkinje cells) suggests that the cerebellar system requires competition between agonist and antagonist microcomplex outputs. This, in turn, suggests the existence of neurones encoding an increase in 'flexor' synergy motor command, while others encode an increase in 'extensor' synergy motor command. Because some experimental data suggest that nuclear cells are joint-specific (as reviewed in the companion paper), and because the present model uses an arm model with two degrees of freedom, four microcomplexes were implemented: two controlling muscle synergies around the shoulder and two for the elbow, thus modelling four functionally distinct groups of nuclear cells. Each group (three cells

‡By not taking into account the climbing fibre afferents either in the Purkinje cell or in the nuclear cell equation, we implicitly make the following assumption: the climbing fibres send collaterals to the deep nuclei on their way to the cerebellar cortex; the excitation of the interpositus neurones by these collaterals would nullify the strong inhibition caused by the complex spikes, which are the response of the Purkinje cells to the climbing fibre firing.

per group) projected to a functionally distinct group of cortico-spinal cells that controlled either an extensor or a flexor synergy. Because inputs from both agonist and antagonist muscles affect the excitation of the same cells, half the nuclear cells receive collaterals from all the mossy fibres carrying information related to one joint (including the bi-articular muscle information). To account for the phasic nature of the nuclear cell firing, only velocity signals were assumed to be summed at the nuclear cell level. The membrane potential of each nuclear cell is given by:

$$\tau_{nu}\frac{d\,nu(i)}{dt} = -nu(i) - \sum_j w_{pc\_nuc}PC(j) + w_{mf\_nuc}\sum_k (MF\_sens(k) + MF\_des(k)) + B_{nu}, \quad (12)$$

where B_{nu} is the background *Mf_sens* and *Mf_des* are mossy fibre activity from sensory and central (descending) origins, respectively. w_{pc_nuc} represents the strength of the Purkinje cell inhibition and w_{mf_nuc} the strength of the mossy fibre collaterals. The nuclear cell firing rate was derived via a ramp function.

Cerebellar learning

The companion paper suggests that IO cells detect torque-like errors in performance. In the present model, the error in motor performance around a joint was separated into a positive error (error due to a flexor) and a negative error (error due to an extensor). For each joint, there were two groups of IO cells, and, thus, four groups innervating four microcomplexes (three cells per group). For the shoulder:

$$Error(t) = K_p(\theta_d(t) - \theta_r(t)) + K_v(\dot{\theta}_d(t) - \dot{\theta}_r(t)) + K_a(\ddot{\theta}_d(t) - \ddot{\theta}_r(t)) \quad (13)$$

$E_{flex} = Error(t)$ if $Error(t) > 0$, zero otherwise
$E_{ext} = -Error(t)$ if $Error(t) < 0$, zero otherwise,

where the subscript *d* refers to the delayed desired trajectory from central origin and the subscript *r* refers to the delayed actual trajectory. The actual acceleration (delayed by 10 ms in the model) may be provided by the Golgi tendon receptors (because they sense muscle tension, which is related to acceleration) and the actual velocity and position by the muscle spindles. Because the IO cells fire at a very slow rate, they were modelled as spiking neurones. An IO spike is represented as $IO = 1$, while *hyper* is the hyperpolarization following a spike. This hyperpolarization brings *io*low threshold again.

$$\text{If } io(t) = \theta, \text{ then } io(t+\delta) = \theta\text{–}hyper, \text{ and } IO(t+\delta) = 1, \text{ for } 0 < \delta \leq d, \quad (14)$$

where θ is the threshold for an IO spike and *d* the duration of a spike. Otherwise:

$$\tau_{lo}\frac{dio}{dt} = -io + E + noise. \quad (15)$$

The term *E* is either E_{ext} or E_{flex} and, along with the added noise term, ensures that the larger the amplitude of the error, the higher the probability that the IO cell will fire.

Houk *et al*. (1990) developed a model of the cerebellum in which a neurochemical model of LTD was proposed. Schweighofer *et al*. (1996a) refined this detailed neurochemical modelling by introducing the 'window of eligibility' to account for timing issues in cerebellar learning. The present cerebellar model included this LTD modelling. Note that a learning rule containing only a LTD term is not possible because all the weights would soon be zero. Consequently, a subtractive normalization term was included in the learning rule to keep the sum of the weights constant for each Purkinje cell.

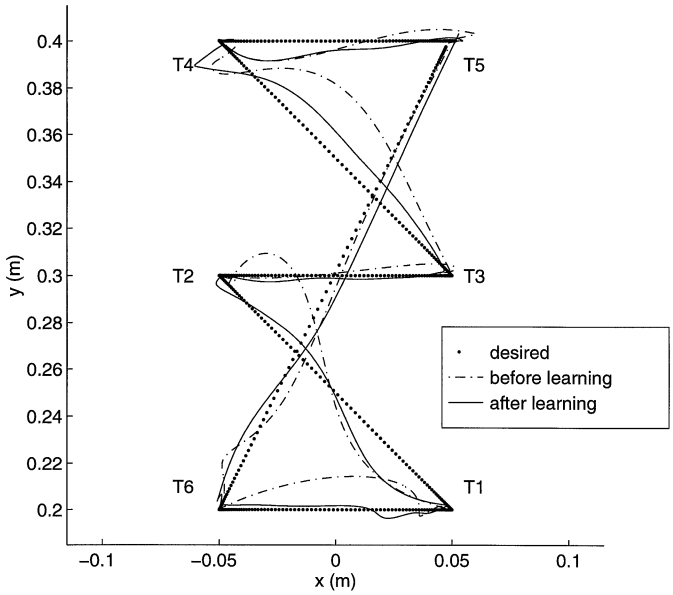

FIG. 2. Arm trajectories before learning and after 2000 trials in a Holmes-like experiment for 750 ms movements. Note how the real trajectory was closer to the planned trajectory after learning.

Results

The cerebellar model was first tested in the control of the arm in a set of experiments similar to those of Holmes (1939). First, the learning rate parameters were varied and good learning was observed for the learning rate α set at 3×10^{-6} and for the two eligibility time constants set at 50 ms (see Schweighofer *et al*., 1996a; simulations showed good performance of the system for eligibility time constants up to 150 ms). In Figure 2, the movements shown have a duration of 750 ms. Comparison of the trajectories before learning and after 2000 training movements illustrates how the cerebellum learned to compensate for the interaction torques. The trajectories were straighter and the actual trajectories were much closer to the planned trajectories, especially in those movements which involved significant rotation of both joints (i.e. T6 => T1, T1 => T2 and T3 => T4). To quantify learning, the mean square error (MSE) was measured between the desired trajectory delayed by 30 ms (which corresponded to the spinal cord delay) and the real trajectory during the six movements. In Figure 2, before learning the MSE was 3.51 and after learning it was 0.62. The learning curve for 2000 movements (duration of 1 sec) is shown in Figure 3. In this case the MSE is reduced by a factor of about 7.

The activity of the different neurones of the cerebellar network were recorded during a 1 second movement from T3 to T4 both before learning and after 2000 training movements (this movement involves significant rotation of both the shoulder and the elbow joints). As recorded experimentally (Van Kan *et al.*, 1993), the mossy fibres in the model carried either a mixture of delayed real position and velocity or a mixture of desired position, velocity and acceleration. The granule cells exhibited a large variety of responses and many cells were silent for this particular movement. This variability suggests that these cells provided Purkinje cells with a large training context, as hypothesized by Albus (1971). Because at least two mossy fibres are necessary to activate a granule cell and the cells are strongly inhibited by Golgi cells,

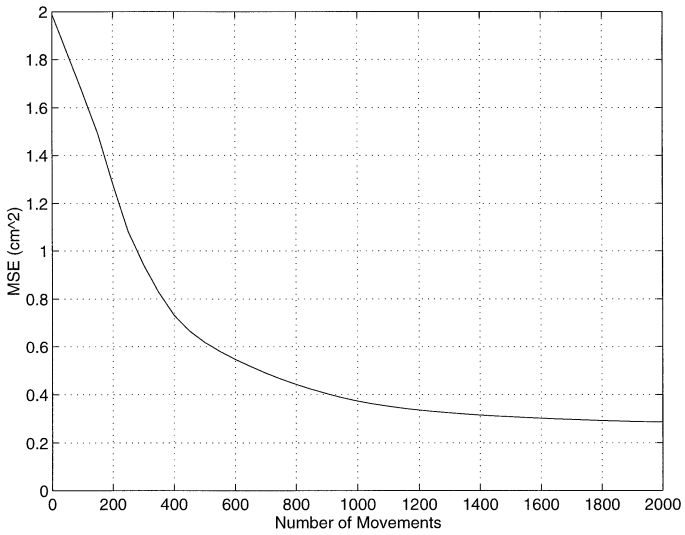

FIG. 3. Learning curve corresponding to learning the movements shown in Fig. 2 with a longer duration (1 s). The mean square error (MSE) was calculated from an evaluation set of six movements every 100 movements.

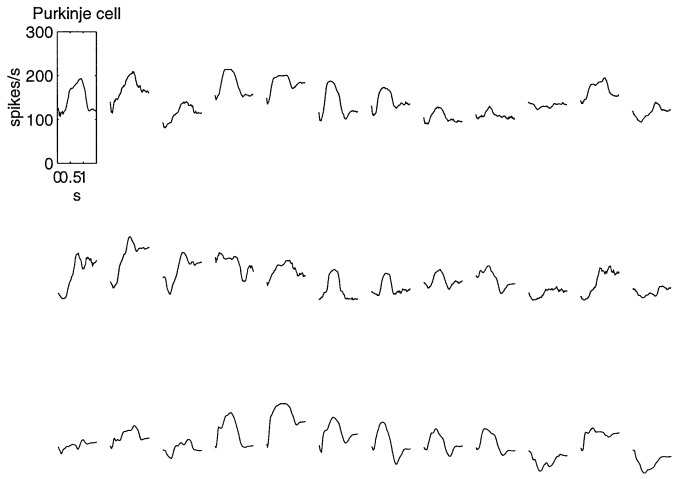

FIG. 4. Purkinje cell firing rates after learning (movement duration: 1 s). The responses are different along the same parallel fibre for the following reasons: first, the inputs are not from the same parallel fibre population; second, there is a decrease of the number of synapses along the parallel fibres; third, several ascending granule cell synapses connect the overlying Purkinje cell; and fourth, the climbing fibres innervate the Purkinje cells perpendicularly to the parallel fibre and therefore affect the learned state of each Purkinje cell in a different manner.

the membrane potential of many granule cells is below threshold for a given movement. The activity of some cells appears to correlate with position, velocity, and acceleration, but for most cells, the Golgi inhibition added new dynamics to the granule cell firing. Because Golgi cells receive so much convergent information from both mossy and parallel fibres, their low firing rates do not correlate in a straightforward manner with any movement variables. Their generally unimodal shape conveys undifferentiated inhibitory signals that dampen the underlying granule cell activity. The firing rates of the modelled cells were very similar to those recorded in the monkey by Van Kan *et al.* (1993).

Figure 4 shows the activity of Purkinje cells after learning. Due to strong local inputs and a variety of inhibitory influence from basket cells, the cells exhibited diverse activity before learning. After learning, the firing rate was greatly reduced. Although no clear correlation between Purkinje cell activity and any variable of the movement emerges from these results, learning may capture the interaction torque by 'shaping' the Purkinje cell firing such that the underlying nuclear cell activity relates to compensatory torques signals.

Fortier *et al.* (1989) showed that many Purkinje cells generate signals that vary with the direction of movement of the proximal arm during aimed reaching movements, suggesting that these cells have a role in the control of the muscle groups generating these movements. To test the present model for directional tuning of this type, simulations of reaching to eight targets spaced at 45° around a circle with a radius of 20 cm, with a movement duration of 1.1 s were performed. The MSE was reduced from 4.54 to 1.36 after 2000 movements, indicating that these movements were more varied and that learning to control them was a more difficult task than that illustrated in Figure 2. Figure 5 illustrates the activity of a simulated Purkinje cell exhibiting directional tuning during reaching movements to the eight targets from the central position. Some other cells did not exhibit directional tuning and many cells in the model cannot really be classified as being directionally tuned or not, since all the ranges are seen. However, the average firing rate for all the cells combined in each direction varied between 92 and 109 spikes per s; thus the eight directions were approximately equally represented. Directional tuning of individual Purkinje cells was an emergent property of the model because before learning no significant directional tuning was observed.

Nuclear cell activity after learning is shown in Figure 6. There were four groups of three cells, each controlling one joint 'synergy'. The difference in the sum of activity from the first three cells and cells 4, 5, and 6 affect the shoulder torque. For this particular movement, the Purkinje cells 'shape' nuclear cell activity such that the first three nuclear cells tend to fire in the earlier part of the movement and the next three in the later part of the movement (the opposite is true for the six 'elbow' cells). Before learning, the net influence of the cerebellum on the activity of the reaching circuitry was near zero; thus, the trajectories obtained without the cerebellum and with a naive cerebellum are similar. During training, however, cerebellar influence became either positive or negative, depending on the direction of the error. An overshoot of a joint movement increased the extensor microcomplex output and an undershoot increased the flexor microcomplex output. This suggests that the adaptive reaching system requires not just simple gain control, but adaptation of coordination between the different reach generators.

The IO spikes are shown in Figure 7(a) before learning and in Figure 7(b) after learning. The number of IO spikes dramatically decreased after learning because the error in trajectory decreased significantly, due to cerebellar activity. Figure 8 illustrates the average effect of learning on the IO firing rate. Before learning, there were two peaks of activity, in the early and the late phase of the movement. After learning, only the early excitation remained.

One important property of neural networks is the ability to generalize. After learning to perform some movements accurately, the system should then be suited for another set of movements. To test if the present model generalizes, the results of the learning experiments shown in Figures 2 and 3 were compared with experiments using similar movements with an x and y deviation for 1 s movements. The relative error (MSE after learning divided by the MSE before learning) is plotted in Figure 9. The curve is smooth (the minimum value with no deviation is 0.138) and for almost all the values considered, the relative error is below 0.5.

Three additional parameters of the model were also tested. First, because signals in the nervous system are often noisy, the present model was tested for robustness to noise by varying the sensory mossy fibre noise level. Second, the present model was compared to Fujita's

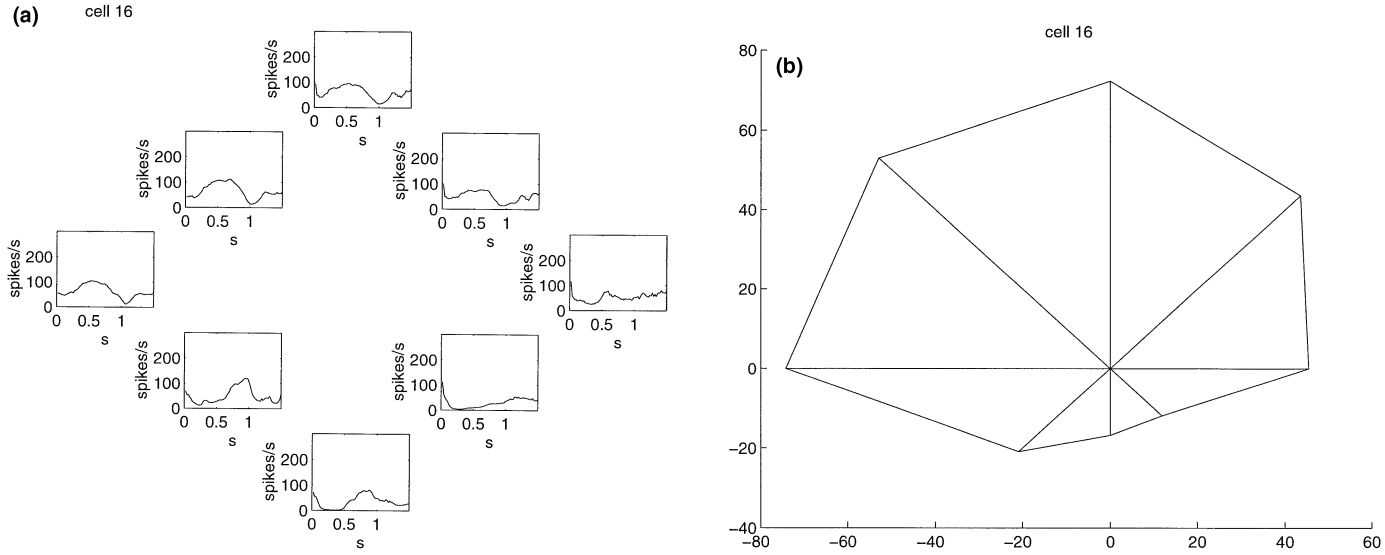

FIG. 5. Directional tuning of a Purkinje cell after learning recorded during reaching in 1.1 s from the central position to eight targets arrayed at 45° intervals around a circle with a radius of 20 cm. (a) The firing rate of the cell during each movement is displayed in the same location as the target. (b) Activity of the cell displayed as a polar plot. The length of each axis represents the mean cell activity of the cell during the first half of the movement to the corresponding target.

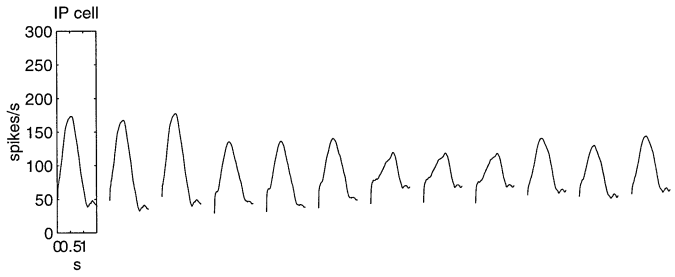

FIG. 6. Nuclear cell firing rates after learning (movement duration: 1 s). Long-term depression occurring in overlying microzones (composed of nine Purkinje cells) allowed the nuclear cells to fire in the learned state. Nuclear cells can therefore provide the needed corrective motor command.

cerebellar model (1982). Fujita posited that Golgi cells have large time constants (in the order of 10 s) giving rise to a large range of phase leads and lags in granule cells. Finally, the impact of the parallel fibre length on the performance of the model was assessed. The best performance (MSE = 0.34) was obtained with a mean mossy fibre noise of 10 spikes/s, parallel fibre length of 30 units, and a Golgi synapse time constant of 0.01 s. Figure 10(a) shows that the model was very accurate with a large range of mossy fibre noise, even with high noise levels. Second, for mean values of the Golgi cell synapse time constants up to 200 ms, the model was very robust. With larger time constants, however, the learning performance was poor (Fig. 10b). Finally, when parallel fibre length from 0 to 30 units was tested, as predicted, only long parallel fibres allowed proper learning, that is, proper coordination (Fig. 10c). If the parallel fibres were short, the Purkinje cell inputs originated mostly from the same joint and many terms of the inverse dynamics equation could not be computed. There is an appropriate balance between inputs from one joint and other joints when the parallel fibres were long enough.

Discussion

The present study utilized a novel, large cerebellar model based on the microcomplex hypothesis proposed by Ito (1984) to examine the role of the cerebellum in the coordination of movement. The model was tested with realistic input delays derived from the functional model proposed in the companion paper. The results indicate that a realistic cerebellar network could learn a part of the inverse dynamics for an arm model containing a redundant set of muscles. Despite both realistically low IO firing and noisy mossy fibre inputs, the cerebellum greatly improves the performance of the controller and exhibits good generalization. The responses of the different cell groups compare favourably with available physiological data and the modelled Purkinje cells exhibit directional tuning after learning, as has been shown experimentally. Furthermore, the results indicate that the parallel fibres, due to their long lengths, provide the Purkinje cells with the appropriate variables to learn the inverse dynamics internal model.

The influence of the climbing fibre signals on the Purkinje cell simple spikes is still highly debated (Simpson *et al.*, 1996). First, IO spiking is often observed in relation to the onset of movement (Mano *et al.*, 1986; Welsh *et al.*, 1995; Keating & Thach, 1995). Consideration of the effects of the complex spike on subsequent simple spike activity led several researchers (Mano *et al.*, 1986; Llinás, 1991) to propose the synchronizing pulse hypothesis. Under this hypothesis, the role of the climbing fibre is to assist the effective onset of the movement or even to allow the movement to occur. Because a transient, short-lasting pause of simple spike activity is often observed after an IO spike (Mano *et al.*, 1986; Sato *et al.*, 1992), and because IO cells are electrotonically coupled, IO activity at the onset of the movement may reduce Purkinje cell inhibition of nuclear cells and thus allow the initiation of the movement. Another hypothesis concerning the role of the IO is commonly known as the Marr (1969) and Albus (1971) hypothesis. This hypothesis is supported by experiments showing that during adaptation of limb movement, complex spike discharge increases dramatically in frequency and temporal relation to movement, only to return to lower frequencies when adaptation is complete (Gilbert & Thach, 1977; Ojakangas & Ebner, 1992). But as Keating & Thach (1995) note, this hypothesis appears to be inconsistent with the fact that complex spikes continue to occur in strong correlation with the beginning of the movement. The results of the present study may help resolve this issue. The IO spikes may carry the information required to learn complex internal models, despite their very low firing rates. The second peak of IO

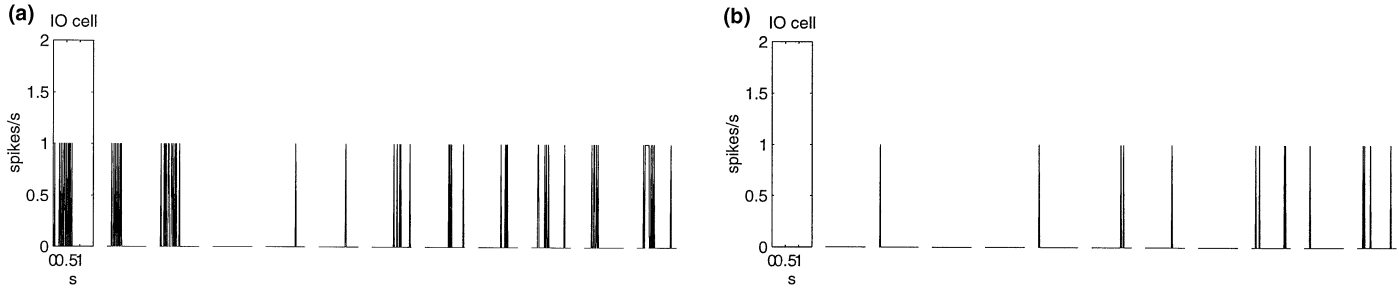

FIG. 7. Inferior olive cells responses (a) before and (b) after learning (movement duration: 1 s). The number of spikes was much reduced after learning.

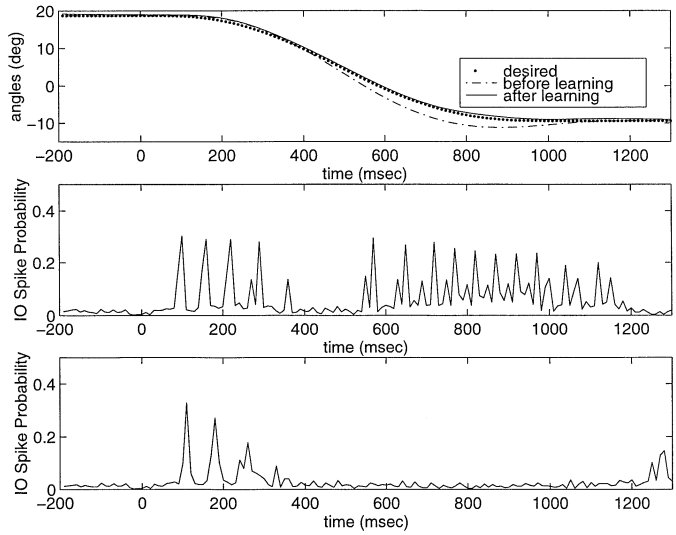

FIG. 8. Effect of learning on inferior olive (IO) cell responses (movement duration: 1 s). (a) The movement trajectory was more accurate after learning. (b) Average IO cell responses related to the six shoulder cells for 50 T3 = > T4 movements before learning. (c) Average IO responses after learning: only some early excitation remained.

activity disappeared after learning, as predicted by Marr and Albus and first reported by Gilbert and Thach. The first peak does not disappear because the IO compares the desired trajectory with the delayed real trajectory. Because of the delays, the error in position is quite small, but the acceleration error is such that the IO cells fire consistently at the beginning of the movement. Despite this early activity, however, the results of the present study show that learning is stable and maintained. This suggests that the IO spike at the beginning of the movement is inevitable, but not important functionally.

Extensions of the model

The present model incorporated a very large number of anatomical, physiological and neurochemical data. Some important features of cerebellar organization were simplified, however, and further even more comprehensive models should incorporate the features listed below. (i) The mossy fibre inputs likely carry a much richer set of information than that modelled, for example, postural information, vestibular information, desired motor commands, visual information, recurrent connections from several brainstem nuclei, and also a 'mental set' corresponding to the significance of the movement and the desired performance. (ii) Although the model was large enough to give strong predictions on learning capability and information processing in the cerebellar cortex, the number of cells included was limited to make the model computationally tractable. The role of the basket cells was not thoroughly analysed because the 'width' of the modelled cerebellum was only three cells, much less than in the cerebellum. Moreover, the stellate cells acted as a simple feedforward inhibition mechanism. (iii) The learning capabilities of the present model were not optimal (small movements at low speeds), suggesting that the three following processes should be developed: (a) a more efficient, and biologically plausible learning rule; (b) more extensive non-linear processes in the Purkinje cell dendrites in order to learn how to compensate for the (non-linear) interaction torques at higher speeds and (c) a better representation of the inputs at the granule cell level.

Finally, for an arm with redundant degrees of freedom, there are innumerable possible trajectories and a desired trajectory is formed in the nervous system by optimizing some criterion. The arm modelled in the present study only included two degrees of freedom, compared to seven in a human arm. Once the trajectory is generated, expansion of the present model to control an arm with three or more degrees of freedom is quite straightforward, although it would be computationally intractable with present computers.

Testable predictions

The results of the companion paper and the present paper, lead to the prediction that the cerebellum gradually learns part of the inverse model of the plant: the non-adaptive pathway is an approximate inverse model that is adaptively compensated for by the cerebellum. After training, the cerebellum output is determined by the training signal, that is, IO firing. Thus, a strong prediction of the model is that the computation performed by the IO cells (or by some cells projecting to the IO) should be similar to equation 13, that is, it should correlate with both desired and actual position, velocity, and acceleration. Kobayashi *et al*. (1995) analysed the firing rates of climbing fibre inputs to the Purkinje cells in the ventral paraflocculus by measuring the complex spike activity during ocular following responses. Using the inverse dynamics representation model, these authors found that the complex spike instantaneous firing rates correlate with acceleration, velocity, and position. This leads to the prediction that IO firing rates during arm movements may be represented with equation 13.

LTD allows only a unidirectional functional change. To generate adaptation in both directions for each joint, four microcomplexes were implemented in the present model: two controlling muscle synergies around the shoulder and two for the elbow. We predict the existence of neurones encoding an increase in 'flexor' synergy motor command, while others encode an increase in 'extensor' synergy motor command.

The results concerning the mean time constant of the Golgi cell synapses indicated that this value should not exceed 1 s for arm reaching movements. Fujita (1982), however, predicted that this time constant should be in the order of 10 s for the vestibulo-ocular reflex system.

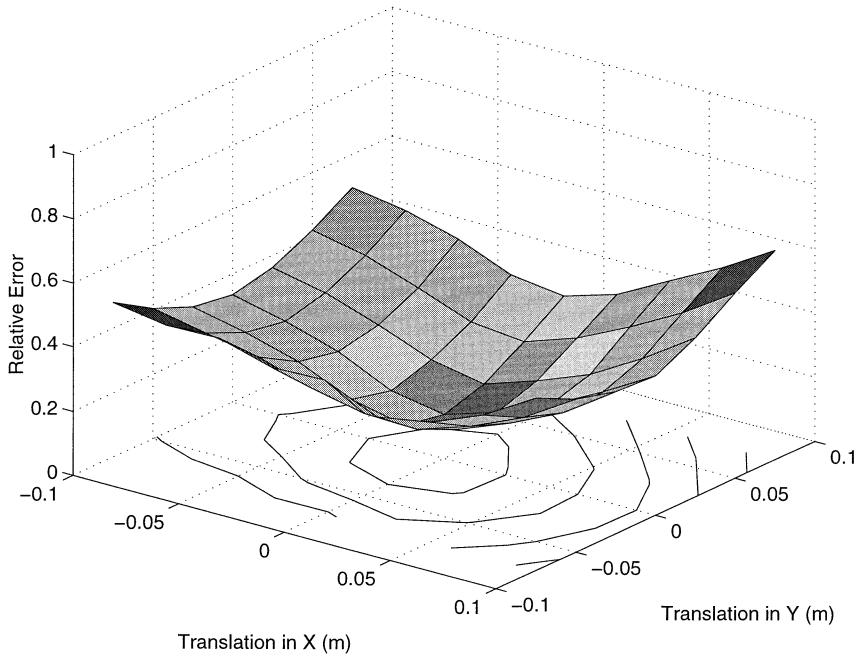

FIG. 9. Generalization properties of the network. The relative error [mean square error (MSE) after learning divided by the MSE before learning] from the experiments illustrated in Fig. 3 is plotted as a function of the translation between the original learned movement set and the test set. Note how the curve is smooth and that for almost all the values considered the relative error is below 0.5. The contour plot has an increment of 0.1 and the minimal value, for no deviation, is 0.138.

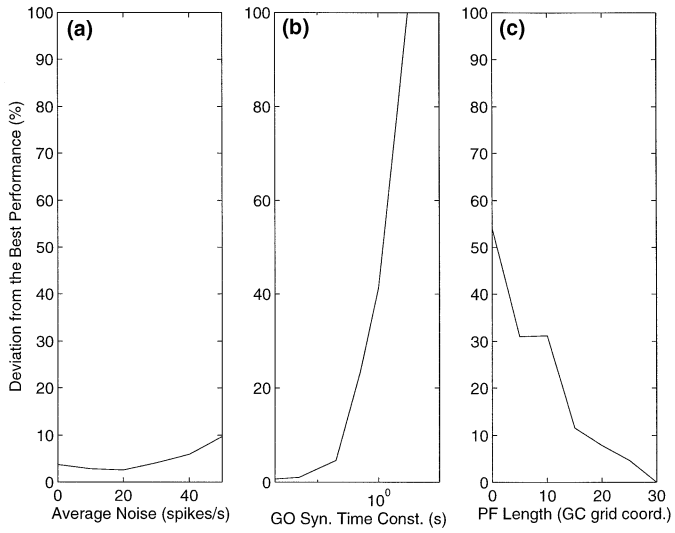

FIG. 10. Deviation from the best results with Holmes-like target, individual movement duration: 1 s for 2000 movements. (a) Mean square error (MSE) is plotted as a function of sensory mossy fibre noise. The model is robust to a large level of mossy fibre noise. (b) MSE of the Golgi synapse mean time constant – the standard deviation is kept at 1/10th of the mean. Fujita proposed that the duration of Golgi cell inhibition is in the order of several seconds. This graph shows that, for acceptable learning of arm control, the mean time constant should be at most 100 ms (semilog graph.) (c) We then vary the parallel fibre length parameter from 0 to 30 units of granule cell grid. If the parallel fibres were too short, the Purkinje cell inputs originated mostly from the same joint via ascending granule cell synapses and it was not possible to compute many terms of the inverse dynamics equation. Only when the parallel fibres were long enough was there the appropriate balance between same joint and other joint inputs

Recording experiments may reveal if the time course of the Golgi-cell inhibition can vary, in a system-dependent manner.

Finally, the present study demonstrated that modelled IO cells had two peaks of activity: an early one related to the onset of movement and due to the delay between the desired and the actual trajectories and a later one that disappeared after learning. This leads to the prediction that the average activity of a group of IO cells related to arm reaching would yield similar results in an adaptation task (e.g. wrist movements against a variable load); before learning, two peaks of activity should be observed, while after learning, only an early peak should be observed.

Acknowledgements

We thank Kenji Doya for his helpful comments during the development phase of the model. This research was supported in part by Grant NOOO14-92-J-4026 from the Office of Naval Research for research on ‘Cerebellum and the Adaptive Coordination of Movement’, in part by ATR, and in part by a Human Frontier Science Program grant to Mitsuo Kawato.

Abbreviations

IO	inferior olive
LTD	long-term depression
MSE	mean square error

References

Albus, J.S. (1971) The theory of cerebellar function. *Math. Biosci.*, **10**, 25–61.

Bartha, G. (1992) *A Computer Model of Oculomotor and Neural Contributions to Conditioned Blink Timing*. PhD Dissertation, Los Angeles, USC.

Bastian, A.J., Martin, T.A., Keating, J.G. & Thach, W.T. (1996) Cerebellar ataxia: abnormal control of interaction torques across multiple joints. *J. Neurophysiol.*, **76**, 492–509.

Berthier, N.E., Singh, S.P., Barto, A.G. & Houk, J.C. (1993) Distributed

representation of limb motor programs in arrays of adjustable pattern generators. *J. Cogn. Neurosci.*, **5**, 56–78.
Boylls, C.C. (1975) A theory of cerebellar function with applications to locomotion. *Coins Tech. Rep*., **75C-6**.
Cheney, P.D. & Fetz, E.E. (1980) Functional classes of primate corticomotorneural cells and their relation to active force *J. Neurophysiol.*, **44**, 773–91.
Eccles, J.C., Ito, M. & Szent_gothai, J. (1967) *The Cerebellum as a Neuronal Machine*. Springer-Verlag, New York.
Evarts, E.V. (1966) Pyramidal tract activity associated with a conditioned hand movement in the monkey. *J. Neurophysiol.*, **29**, 1011–27.
Fortier, P.A., Kalaska, J.F. & Smith, A.M. (1989) Cerebellar neuronal activity related to whole arm reaching movements in the monkey. *J. Neurophysiol.*, **62**, 198–211.
Fujita, M. (1982) Adaptive filter model of the cerebellum. *Biol. Cybern.*, **45**, 195–206.
Garwicz, M. & Andersson, G. (1992) Spread of synaptic activity along parallel fibers in cat cerebellar anterior lobe. *Exp. Brain Res.*, **88**, 615–22.
Gilbert, P. & Thach, W.T. (1977) Purkinje cell activity during motor learning. *Brain Res.*, **128**, 309–28.
Holmes, G. (1939) The cerebellum of man. *Brain*, **62**, 1–30.
Houk, J.C., Singh, S.P., Fisher, C. & Barto, A.G. (1990) An adaptive sensorimotor network inspired by the anatomy and physiology of the cerebellum. In Miller, W. T. (ed.), *Neural Networks for Control*. MIT Press, Cambridge MA.
Ito, M. (1984) *The Cerebellum and Neuronal Control*. Raven Press, New York.
Kawato, M., Furukawa, K. & Suzuki, R. (1987) A hierarchical neural network model for control of learning of voluntary movement. *Biol. Cybern.*, **57**, 169–85.
Kawato, M. & Gomi, H. (1992) The cerebellum and VOR/OKR learning models. *Trends Neurosci.*, **15**, 445–53.
Keating, J.G. & Thach, W.T. (1995) Non-clock behavior of inferior olive neurons: interspike interval of Purkinje cell complex spike discharge in the awake behaving monkey is random. *J. Neurophysiol.*, **73**, 1329–40.
Kobayashi, Y., Kawano, K., Inoue, Y., Takemura, A., Shidara, M., Gomi, H., Kawato, M. (1995) Inverse-dynamics representation of complex spikes discharges of Purkinje cells in monkey cerebellar ventral paraflocculus during ocular following responses. *Soc. Neurosci. Abstr.*, **21**(11–16Nov.), 140.
Llinás, R. (1991) The non-continuous nature of movement execution. In Humphrey, D.R. and Freund, H.J. (eds), *Motor Control: Concepts and Issues*. J Wiley & Sons Ltd, Chichester.
Llinás, R., Baker, R. & Sotelo, C. (1974) Electrotonic coupling between neurons in cat inferior olive. *J. Neurophysiol.*, **37**, 560–71.
Mano, N., Kanazawa, I. & Yamamoto, K. (1986) Complex spike activity of cerebellar Purkinje cells related to wrist movement in monkey. *J. Neurophysiol.*, **56**, 137–58.
Marr, D. (1969) A theory of cerebellar cortex. *J. Physiol.*, **202**, 437–70.
Miall, R.C., Weir, D.J., Wolpert, D.M. & Stein, J.F. (1993) Is the cerebellum a Smith Predictor? *J. Motor. Behav.*, **25**, 203–16.
Ojakangas, C. & Ebner, T.J. (1992) Purkinje cell complex and simple spike changes during a voluntary arm movement learning task *J Neurophysiol.*, **6**, 2222–36.
Oscarsson, O. (1980) Functional organization of olivary projection to the cerebellar anterior lobe. In Courville, J. and Lamarre, Y. (eds), *The Inferior Olivary Nucleus: Anatomy and Physiology.* Raven Press, New York, pp. 279–289.
Sato, Y., Miura, A., Fushiki, H. & Kawasaki, T. (1992) Short term modulation of cerebellar Purkinje cell activity after spontaneous climbing fiber input. *J. Neurophysiol.*, **68**, 2051–62.
Schweighofer, N., Arbib, M.A. & Dominey, P.F. (1996a) A model of the cerebellum in adaptive control of saccadic gain I. The model and its biological substrate *Biol. Cyber.*, **75**, 19–28.
Schweighofer, N., Arbib, M.A. & Dominey, P.F. (1996b) A model of the cerebellum in adaptive control of saccadic gain II. Simulation results. *Biol. Cyber.*, **75**, 29–36.
Schweighofer, N., Arbib, M.A. & Kawato, M. (1998) Role of the cerebellum in reaching movements in humans. I. distributed inverse dynamics control. *Eur. J. Neurosci*, **10**, 86–94.
Simpson, J.I., Wylie, D.R. & De Zeeuv, C.I. (1996) On climbing fibers and their consequences. *Behav. Brain Sci.*, **19**, 384–98.
Thach, T., Goodkin, H. & Keating, J. (1992) The cerebellum and the adaptive coordination of movement. *Annu. Rev. Neurosci.*, **15**, 403–42.
Thompson, R. (1986) The neurobiology of learning and memory *Science*, **233**, 941–7.
Van Kan, P.L., Gibson, A.R. & Houk, J. (1993) Movement-related inputs to intermediate cerebellum of the monkey. *J. Neurophysiol.*, **69**, 74–94.
Welsh, J.P., Lang, E.J., Sugihara, I. & Llinás, R. (1995) Dynamics organization of motor control within the olivarycerebellar system. *Nature*, **374**, 453–7.

Appendix 1. Neural layers and neurone dynamics

In this paper we adopted the cerebellar neuronal model used by Boylls (1975). The major neural elements are two-dimensional neural surfaces, representing mossy fibres, glomeruli, granule cells, Golgi cells, basket cells, stellate cells and Purkinje cells and one-dimensional arrays representing interpositus cells and IO cells. We refer to these neural surfaces as layers. These layers represent the corresponding brain region with the topographic mapping of the region flattened into a plane. To limit 'edge effects', each layer is represented as a 'doughnut': the left side of a layer connects with the right side and the upper side connects with the lower side.

The cells interact only via their 'firing rates' and the firing rate of a cell depends only on its own membrane potential. The simulation cycles through two steps.

Step 1. Updating the membrane potentials. The membrane potential of each cell is described by a leaky integrator equation of the form:

$$\tau_m \frac{dm}{dt} = -m + \sum_k w_e(i)\, EXC(i) - \sum_k w_h(i)\, INH(i)\,,$$

where m denotes the membrane potential of that cell at time t, is the time constant for the rate of change of this potential, while the last two terms are the weighted sum of the excitatory and inhibitory inputs, respectively. The simulations use the Euler method, the simplest approach to solving differential equations. The time step dt is chosen equal to 5 ms and dm/dt is approximated by the ratio $(m(t + \Delta t) - m(t))/\Delta t$ to obtain the difference equation.

Step 2. Updating the firing rates. Rather than model spike generation, a coarse approximation is used (except for the IO firing). The 'firing rate' of a cell is obtained by passing the membrane potential through a sigmoidal or 'squashing' function, unless otherwise specified. The result of the sigmoid transformation is that the firing rate of the neurone increases as the membrane potential increases, up to a specified maximum, at which the firing rate saturates. With G the maximum firing rate, a the slope value, and T the threshold value

$$F_{(m)} = \frac{G}{1 + \exp(-(am + T))}$$

Appendix 2. Parameters used in the model

The neuronal models described above reproduce realistic firing rate time courses, but do not constrain the absolute values of the membrane potential. Each neuronal cell population receives and sends a characteristic set of connections with characteristic convergence and divergence. Anatomical data often give an approximation of these values, as well as quantitative values for the neurone ratio of one cell population to another. In our simulation the number of modelled neurones is limited (e.g. there are 10^{11} granule cells in the human cerebellum, but simulations including more than a few thousand are computationally intractable), however, the ratios of cell types are maintained as much as possible. Once a neuronal population has been determined to be inhibitory or excitatory (this is well known for the cerebellum), the set of parameters to be determined for each neuronal population comprises the time constant, different synaptic efficacies, firing threshold, and slope of the linear portion of the squashing function. Bartha (1992) compiled physiological values for the time constants and baseline firing rates for many cells of the cerebellum. Typical neural responses also give some indication of the slope of the squashing function. The synaptic weights are important parameters in the neural network model. Because no data are available in most cases, we set many values to fixed values (typically 1) or generate them randomly around a mean value as an additional test of the robustness of the model. The following tables summarize the number of cells (Table 1), the divergence/convergence ratios (Table 2), and the different 'default' parameters used in the model (Table 3).

TABLE 1. Cell ratios in the model

Cell type	Cell ratio
Mossy fibres/glomeruli	1 : 4
Mossy fibres/granule cells	1 : 36
Granule cells/Golgi cells	324 : 1
Granule cells/Purkinje cells	81 : 1
Basket cells/Purkinje cells	1 : 1
Stellate cells/Purkinje cells	1 : 1
Purkinje cells/Golgi cells	4 : 1
Purkinje cells/nuclear cells	3 : 1
Inferior olive cells/Purkinje cells	1 : 3

TABLE 2. Divergence and convergence ratios

Divergence/convergence	Convergence	Divergence
Mossy fibres/glomeruli	16	4
Glomeruli/granule cells	4	36
Glomeruli/Golgi cells	6	4
Parallel fibres/Golgi cells	100	mean = 0.62
Parallel fibres/Basket cells	100	mean = 1.2
Parallel fibres/Stellate cells	100	mean = 1.2
(ascending) granule cells/Purkinje cells	1	1
Parallel fibres/Purkinje cells	720	mean = 7.1
Stellate cells/Purkinje cells	1	72
Basket cells/Purkinje cells	3	3
Purkinje cells/nuclear cells	9	2
Climbing fibre/Purkinje cells	1	3

TABLE 3. Other default parameters of the model

Cell type	No. of cells	Time constant (ms)	Max. firing	Slope	Threshold (and noise)	Synaptic efficacies
Mossy fibre	81 (9∧2)	10	400	0.015	0 (10)	→gc: 0.5 σ = 0.1 →go: 0.15 →nuc: 0.07
Granule cell	2916 (54∧2)	10	200	0.1	−20	→go: 0.01 →ba: 0.05 →stel: 0.05 →pc: LTD
Golgi cell	9 (3∧2)	20	100	0.03	−3	
Golgi cell synapses	324 × 6	0.1 σ = 0.02				→glom 0.6 σ = 0.1
Stellate	36 (12 × 3)	10	300	0.01	−2	→pc: 0.1
Basket	36 (12 × 3)	20	300	0.01	−2	→pc: 0.0005
Purkinje cells	36 (12 × 3)	20	300	0.002	−3	→nuc: 0.2
Purkinje cells dendrites	36 × 72		50	0.5	−3	
Interpositus cells	12 (1 × 12)	10	300	1	−180	→motor spinal: 0.002
Inferior olive cells	12 (1 × 12)	100			1 (1)	